Acta Materialia 171 (2019) 40–47

Contents lists available at ScienceDirect

Acta Materialia

journal homepage: www.elsevier.com/locate/actamat

Full length article

Photovoltage spectroscopy of direct and indirect bandgaps of strained $Ge_{1-x}Sn_x$ thin films on a Ge/Si(001) substrate

S.V. Kondratenko [a, *], Yu.V. Hyrka [a], Yu.I. Mazur [b, **], A.V. Kuchuk [b], W. Dou [c], H. Tran [c], J. Margetis [d], J. Tolle [d], S.-Q. Yu [c], G.J. Salamo [b]

[a] Taras Shevchenko National University of Kyiv, 64 Volodymyrs'ka St, 01601, Kyiv, Ukraine
[b] Institute of Nano Science and Engineering, University of Arkansas, Fayetteville, AR, 72701, USA
[c] Department of Electrical Engineering, University of Arkansas, Fayetteville, AR, 72701, USA
[d] ASM, 3440 East University Drive, Phoenix, AZ, 85034, USA

ARTICLE INFO

Article history:
Received 13 December 2018
Received in revised form
5 March 2019
Accepted 2 April 2019
Available online 4 April 2019

Keywords:
GeSn
Photovoltage (PV) spectroscopy
Strain
Bandgap
Urbach tails

ABSTRACT

The near-bandgap optical properties of $Ge_{1-x}Sn_x$ alloys were characterized by photovoltage spectroscopy and spectral ellipsometry measurements. Contributions of Urbach tailing as well as direct and indirect optical transitions were observed. The compositional dependence of direct bandgaps of strained GeSn films grown on a Ge buffered Si substrate was studied for up to 15% Sn content. The contribution to the photovoltage spectra of $Ge_{1-x}Sn_x$ alloys ($x < 6\%$) from indirect optical transitions was observed at lower energies than from direct bandgaps. Using bowing parameters of $b^{\Gamma}_{GeSn} = 3.16-0.5x$ and $b^{L}_{GeSn} = 1.93$ eV, a correlation was detected between calculated and measured indirect and direct bandgaps at 82 K. As the Sn content was increased, the difference between the energies of the indirect and direct bandgaps decreased, resulting in a smaller contribution of the indirect transitions due to competition with direct transitions and Urbach tails. Two sublayers with different Sn content, strain values and bandgaps were observed for samples with x ~12%. The results indicated that strain relaxation in films with thicknesses exceeding a critical value occurs via formation of a Sn-rich top layer with higher direct bandgap. These findings have important implications when designing IR photodetectors or solar cells.

1. Introduction

Group IV semiconductors, such as Si, Ge, and their alloys, have fundamental limitations against application in optoelectronics owing to their indirect-band nature. In crystalline Ge, the indirect L-valley is positioned only 136 meV below the Γ-valley of the conduction band gap [1], which suggests "directness" owing to $Ge_{1-x}Sn_x$ alloying [2] or a tensile strain of about 2% [3,4]. Increasing the Sn content in $Ge_{1-x}Sn_x$ alloys reduces the conduction band because the edge at the Γ-point lowers more rapidly than that at the L-point, resulting in a crossover from an indirect to a direct bandgap material at critical Sn compositions in the range $6\% < x < 10\%$ [5–7]. Theoretical calculations predict a direct band nature for relaxed $Ge_{1-x}Sn_x$ films with 6.5% Sn, while compressive strain shifts the crossover point to higher concentrations of Sn up to 13% [6,8–10].

The energies of the indirect and direct transitions have been extracted from photoreflectance spectroscopy [11], spectral ellipsometry (SE) [12,13] and photoluminescence (PL) [5,14] measurements. The optical constants of thin films are difficult to determine near the absorption edge for indirect-band GeSn alloys because of the inaccuracy of measured data when the absorption coefficient is $< 10^{-3}$ cm^{-1} due to limitations of SE techniques. Absorption and transmission spectroscopy do not give firmly established bandgap energies owing to differences in the strength of the direct and indirect transitions of about two orders of magnitude, as well as phonon emission and absorption. In PL spectroscopy of samples with low Sn content, two emission peaks corresponding to the indirect and direct transitions have been observed [15]. However, near the predicted indirect-to-direct crossover, PL spectral peaks overlap, hampering accurate determination of the bandgap energies taking into account the filling effect as well as alloy broadening [7]. Whereas absorption, PL spectroscopy and SE techniques have some limitations for accurate study of the indirect transitions,

* Corresponding author.
** Corresponding author.
E-mail addresses: kondr@univ.kiev.ua (S.V. Kondratenko), ymazur@uark.edu (Yu.I. Mazur).

https://doi.org/10.1016/j.actamat.2019.04.004
1359-6454/

photovoltage (PV) spectroscopy can be applied to reveal features of the near-bandgap absorption coefficient spectrum of the $Ge_{1-x}Sn_x$ alloys.

In this work, we report on PV spectroscopy and SE of indirect and direct bandgaps measured in strained GeSn thin films grown on a Ge/Si(001) substrate with different Sn content.

2. Experimental

$Ge_{1-x}Sn_x$ thin films were grown using a commercially available ASM Epsilon reduced pressure chemical vapor deposition reactor. A 700 nm thick strain-free Ge buffer layer was first grown on a Si (001) substrate by a two-step growth method. First, a 150 nm seed layer was grown at < 400 °C in H_2 carrier at a GeH_4 partial pressure of 0.2 Torr then the temperature was increased up to 600 °C. Once the temperature has stabilized at 600 °C, the remaining ~ 500 nm is grown and a post growth in situ anneal is done at > 800 °C. The chamber was then cooled down to <400 °C in H_2, and then the GeH_4 and $SnCl_4$ precursors were introduced into the chamber to initiate the GeSn film growth. GeH_4 and $SnCl_4$ were used as precursors for Ge and Sn, respectively. Depending on required Sn content, the growth temperature was kept in the range from 290 °C to 450 °C. Details of the growth, including the $SnCl_4/GeH_4$ flow ratio, were previously reported [16–20]. All $Ge_{1-x}Sn_x$ thin films were unintentionally doped with a p-type background doping concentration of 10^{17} cm^{-3}.

X-ray diffraction (XRD) measurements were performed using a Panalytical X'Pert Pro MRD diffractometer equipped with a 1.6 kW X-ray tube (vertical line focus) with Cu $K\alpha_1$ radiation (λ= 1.540598 Å) and a symmetric 4 × Ge(220) monochromator. Spectroscopic ellipsometry data were collected using a variable-angle spectroscopic ellipsometer (WVASE32) over the range 0.496–4.768 eV (260–2500 nm) with a resolution of 10 nm at three angles of incidence (65°, 70° and 75°). The absorption coefficient and refractive index data points were obtained by using the Johs-Herzinger model. Spectral ellipsometry and XRD measurements were used to calculate the GeSn layer thickness, Sn composition and strain level. Details of the samples and their properties are presented in Table 1.

To accurately measure optical transitions in the GeSn layers by PV spectroscopy, we fabricated a Au–$Ge_{1-x}Sn_x$-Ge-pSi photovoltaic device. An In/Ga eutectic was scratched into the silicon as a back contact and a gold grid (finger width 100 μm) was evaporated by an electron beam through a shadow mask onto the GeSn films as a front contact. Fig. 1 shows a schematic of the Au–$Ge_{1-x}Sn_x$-Ge-pSi device and rectifying current-voltage (J-V) dependencies. The J-V curves were measured in the dark and under illumination, and PV characterization was carried out with a Picotest 3510A semiconductor analyzer equipped with a preamplifier unit. To characterize the photovoltaic response of the devices, samples were irradiated through the $Ge_{1-x}Sn_x$ layer with excitation energies ranging from 0.4 to 2.0 eV using illumination from a 250 W halogen lamp passed through a monochromator. Spectral dependences were normalized to the constant number of exciting quanta using a nonselective pyroelectric detector.

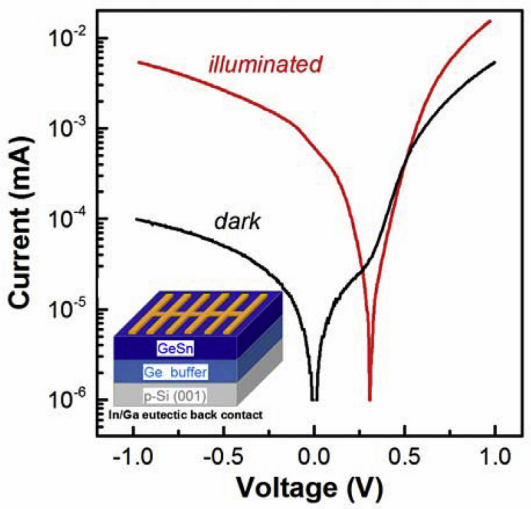

Fig. 1. J-V curves of the Au–GeSn–Ge-pSi device measured in the dark and under illumination with quantum energy of 1.5 eV at 82 K. Inset: schematic of a fabricated Au–GeSn–Ge-pSi structure (the photovoltaic device was contacted by a top evaporated Au grid and a back side scratched In/Ga eutectic).

3. Experimental results

3.1. X-ray diffraction

$\omega/2\theta$ scans around symmetrical Ge (004) Bragg reflection were measured for $Ge_{1-x}Sn_x$ thin films with varying Sn compositions (Fig. 2a). The Si (004) substrate peak (not shown here) was used as a reference for analyzing the $Ge_{1-x}Sn_x$ peaks for each sample. As expected, with increasing Sn composition and incorporation of larger Sn atoms into the Ge lattice, the Bragg peaks from $Ge_{1-x}Sn_x$ shifted to smaller angles due to increases in the out-of-plane lattice

Table 1
The composition, strain, thickness and measured bandgap by photovoltage spectroscopy for $Ge_{1-x}Sn_x$ thin films as a function of Sn content.

No.	Sn (%)	Strain (in-plane, %)	E_0 (eV) from SE	ε_g^{Γ} (eV)	ε_g^{L} (eV)	GeSn film thickness (nm)
A	0	0	0.805	0.880	0.734	300
B	1	−0.02	0.780	0.775	0.683	327
C	3	−0.24	0.744	0.705	0.638	128
D	4	−0.5	0.720	0.674	0.629	70
E	5	−0.67	0.700	0.636	0.594	88
F	6	−0.82	No res	0.611	0.566	96
G	8	−0.8	0.675	0.563	–	90
H	10	−1.16	0.605	0.530	–	59
I	–	–	0.582	0.464	–	45
	11.6	−1.49		0.543		
J	–	–	0.545	0.454	–	100
	11.6	−1.36		0.535		
K	13.7	−0.93	0.509	0.447	–	150
	11.9	−0.67		0.532		
L	14.9	−0.81	0.500	0.425	–	200
	11.8	−0.36		0.505		

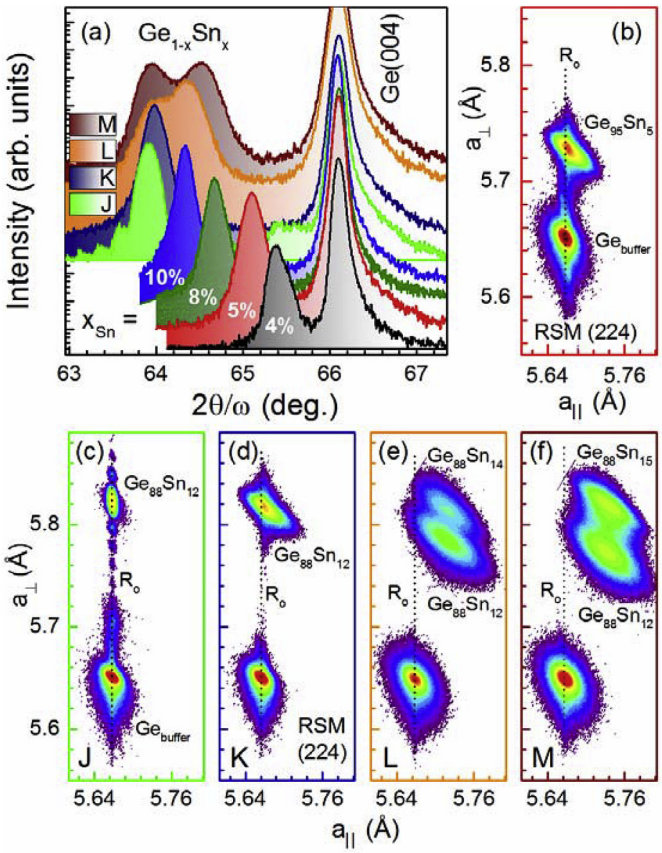

Fig. 2. (a) X-ray diffraction $\omega/2\theta$ scans around symmetrical Ge (004) Bragg reflections for $Ge_{1-x}Sn_x$ thin films with different compositions. (b–f) Reciprocal space maps (RSMs) measured around asymmetrical Ge(-2-24) reflection.

parameter ($a_\perp$) as well as compressive strain in the $Ge_{1-x}Sn_x$ layer induced by the Ge substrate. However, for samples J and K, doublet peaks indicated phase separation, i.e., the $Ge_{1-x}Sn_x$ films consisted of two regions with different strain and composition. This phenomenon was observed earlier and growth mechanisms have been proposed to describe the compressive strain influence on the efficiency of Sn incorporation into Ge lattice sites [18,21].

To estimate the strain and calculate the Sn composition, reciprocal space maps (RSMs) were measured around the asymmetrical Ge(-2-24) reflection. As can be seen in Fig. 2b–d, pseudomorphic growth on the Ge substrate was preserved for $Ge_{1-x}Sn_x$ thin films with a wide range of Sn compositions. However, as soon as the in-plane coherency between the $Ge_{1-x}Sn_x$ film and Ge buffer during the growth was broken, there was a spontaneous change in the composition and strain in the overgrowth layer (see Fig. 2e and f for samples J and K, respectively). The Sn composition and strain state of the $Ge_{1-x}Sn_x$ films were calculated from the following equations (Eqs. (1)–(4)) [22–24]:

$$a_0^{GeSn}(x) = a^{Sn}x + a^{Ge}(1-x) + bx(1-x) \quad (1)$$

$$a_0^{GeSn}(x) = \frac{a_\perp^{exp} + \left(\frac{2C_{12}(x)}{C_{11}(x)}\right)a_\parallel^{exp}}{1 + \frac{2C_{12}(x)}{C_{11}(x)}} \quad (2)$$

$$C_{12/11}(x) = C_{12/11}^{Sn}x + C_{12/11}^{Ge}(1-x) \quad (3)$$

$$\varepsilon_{||} = \left(a_\parallel^{exp} - a_0^{GeSn}\right)\Big/ a_0^{GeSn}, \quad (4)$$

where $a^{Sn} = 6.4892$ Å, $a^{Ge} = 5.6579$ Å, $b = 0.00095$ Å, $C_{12}^{Sn} = 29.3$, $C_{11}^{Sn} = 69.0$, $C_{12}^{Ge} = 48.3$, $C_{11}^{Ge} = 128.5$, and $a_\perp^{exp}$ and $a_\parallel^{exp}$ are the out- and in-plane lattice parameters, respectively, extracted from RSMs.

As can be seen in Table 1, the compressive strain in $Ge_{1-x}Sn_x$ thin films increased as the Sn concentration was increased up to 12%. However, for samples with $x = 12\%$, a spontaneous change in composition was observed with increasing film thickness ˃ 100 nm. Sample K (film thickness ~ 150 nm) consisted of a bottom $Ge_{98}Sn_{12}$ (~0.7% compressive strain) and top $Ge_{98}Sn_{14}$ (~1%) layer. Sample L (200 nm) consisted of a bottom $Ge_{98}Sn_{12}$ (~0.4% compressive strain) and top $Ge_{98}Sn_{15}$ (~0.8%) layer. Thus, the composition of the top $Ge_{1-x}Sn_x$ layer seemed to depend on the strain relaxation of the bottom $Ge_{1-x}Sn_x$ layer. This result agrees with previously reported data [20,21].

3.2. Spectral ellipsometry

For evaluating the optical properties we have first measured SE spectra by using a variable-angle spectroscopic ellipsometer. Fig. 3

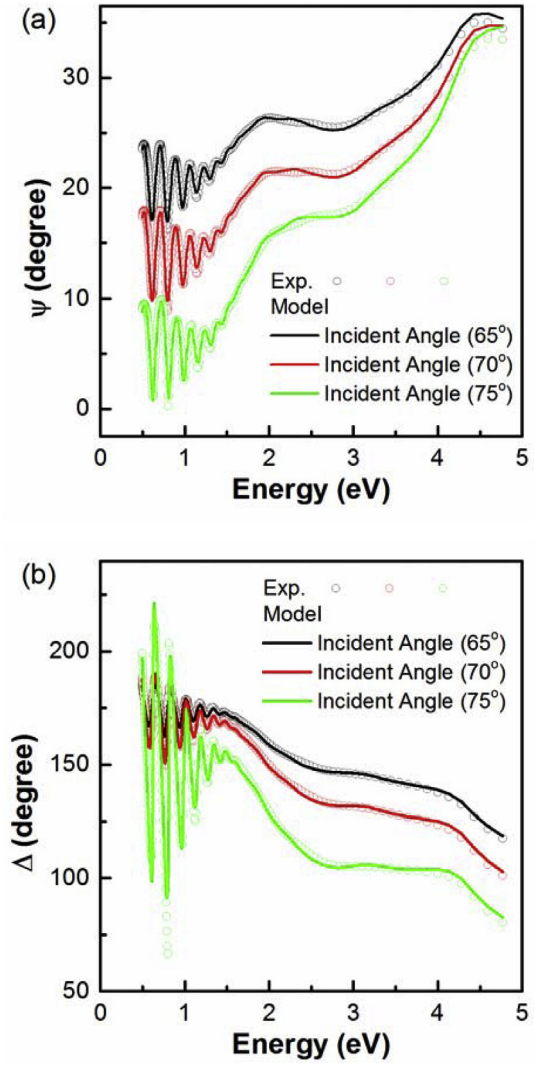

Fig. 3. Angle dependencies of amplitude component ψ(a) and the phase difference Δ (b) for sample I.

shows the measured angle dependencies of the amplitude component (ψ) and phase difference (Δ) for sample I as an example. To obtain the optical constants of GeSn layer, the experimental ψ and Δ spectra were fitted by using the WVASE32® software with Johs-Herzinger parameterized semiconductor model and a joint of five oscillators [25]. A four layer structure was built for data processing, comprising a Si(001) substrate, Ge buffer layer, GeSn thin film and surface rough layer (50% air and 50% GeSn, given by the software). The optical constants for the Ge buffer were fitted and obtained separately, and further used as baseline for other samples. With this information, the estimated thickness and optical constants of the GeSn films, i.e., the real and the imaginary parts of the dielectric function, were obtained for the range 0.496–4.768 eV. Fig. 4 shows the real (ε_1) and the imaginary (ε_2) parts of the pseudo-dielectric function $\langle\varepsilon\rangle$ for the sample G with $Ge_{92}Sn_8$ film. The critical points E_0, associated with the direct transitions in the GeSn films were extracted by fitting of the second derivative of imaginary part of dielectric function using a standard line shapes [26]. It should be noted, that in addition to pseudo-dielectric function, the point-by-point dielectric function were also applied for modeling [27]. However, we found that the point-by-point method give poor signal-to-noise ratio for the spectral region of weak absorption from 0.5 to 1.0 eV and therefore can't be used for the critical point E_0 determination in the studied GeSn films.

Table 1 summarized the critical points for all investigated the GeSn samples. As Sn percentage increases, a red shift in the energy of critical points E_0 due to the direct transitions is observed. The indirect absorption edge was not detected due to the limitations of SE technique in the spectral regions with low absorption coefficient. Therefore, in order to measure the near-bandgap optical transitions in GeSn thin films more accurately, the PV spectroscopy was applied.

3.3. Photovoltage spectroscopy

Fig. 1 shows J-V curves of the Au–$Ge_{1-x}Sn_x$-Ge-pSi device measured in the dark and under illumination with quantum energy of 1.5 eV at 82 K. As can be seen, the dark current in the reverse bias was an order of magnitude lower than in the forward direction. At the same time, illumination shifted the J-V curve due to PV and photocurrent generation. The saturation value of the PV signal for all studied junctions was found to be in the range 0.25–0.50 V for an excitation power of 20 mW/cm^2 at 80 K. This value provides a rough estimate of the potential barrier height for the Au–$Ge_{1-x}Sn_x$-Ge-pSi diode because the PV signal depends nonlinearly on the intensity of illumination and saturates at high-intensity illumination [28]. PV spectroscopy measurements were performed at a low excitation power of 100 μW/cm^2. Under these conditions, the change of barrier height with illumination was expected to be small. Hence, the PV signal could be assumed to be directly proportional to the absorption coefficient and reflect the main features of the optical absorption spectrum.

Fig. 5 shows the spectral dependence of representative PV spectra for Au–$Ge_{1-x}Sn_x$-Ge-pSi devices with Sn concentrations of 0%, 1%, 3% and 12%. Each spectrum was measured at 82 K and comprised a contribution from electron-hole pairs photoexcited in the Si substrate starting from 1.17 eV, a Ge buffer layer with threshold energy for indirect transition at 0.72 eV, and a PV component with an absorption edge at lower energy (in the range $h\nu < \varepsilon_{ind,Ge}$) assigned to both the indirect and direct interband transitions in the GeSn thin films. We also analyzed the PV spectrum edge, where the contribution to the measured signal was due to absorption in the GeSn films alone. The type of interband transition (indirect or direct) was identified by analyzing the shape of the $U_{PV}(h\nu)$ curve in this range. To clarify the contribution of direct transitions to the PV generation and identify the direct bandgaps, spectral dependencies were plotted in $(h\nu U_{PV})^2$-$h\nu$ coordinates. Fig. 6a shows close-ups of the spectral dependencies of $(h\nu U_{PV})^2$ for samples with 1%, 4%, 5%, 8%, 10% and 12% (45 nm) over linear regions used for fitting. Extrapolation to the photon energy axis yielded the direct bandgap, ε_{dir}, for the $Ge_{1-x}Sn_x$ thin films, as marked by arrows in Fig. 6a. For example, PV spectra of the diode with a $Ge_{99}Sn_1$ film contained two linear regions with threshold energies of 880 meV and 775 meV related to direct transitions in the Ge buffer and $Ge_{99}Sn_1$, respectively. The results showed that as the Sn content increased, the direct bandgap shifted toward lower energy due to changes in the electronic band structure of the GeSn alloys.

Below the direct bandgap, $h\nu < \varepsilon_{dir}$, a PV signal was observed due to both indirect transitions and transitions between the tails of density-of-states in the valence band and conduction band of GeSn alloys (Urbach tail). In the case of Urbach behavior of the absorption edge, the spectral dependence of the PV signal can be described by an exponential function:

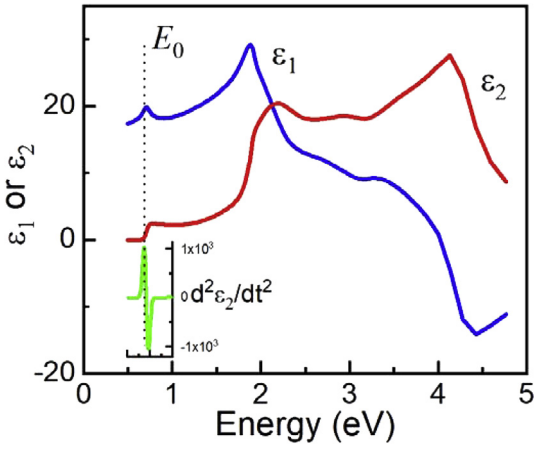

Fig. 4. Real (ε_1) and imaginary part (ε_2) of pseudo-dielectric function obtained from ψ and Δ for the $Ge_{92}Sn_8$ sample. The inset shows numerical second derivative of imaginary part of dielectric function.

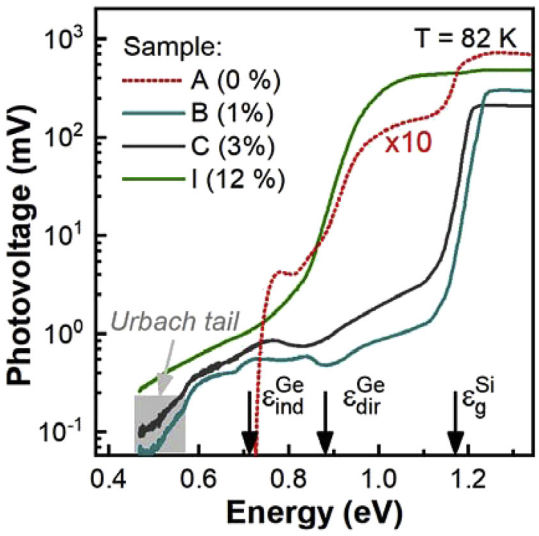

Fig. 5. Spectral dependencies of photovoltage of Au-GeSn-Ge-pSi devices with Sn concentrations of 0%, 1%, 3% and 12%.

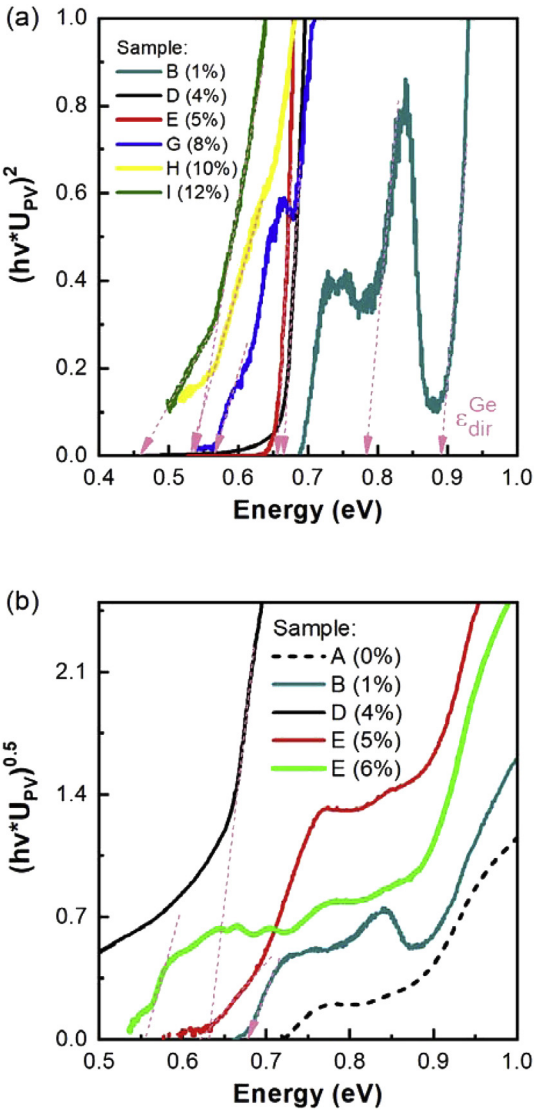

Fig. 6. Close-up of spectral dependencies plotted (a) in $(U_{PV}h\nu)^2$-$h\nu$ coordinates for samples with 1%, 4%, 5%, 8%, 10% and 12% (45 nm), and (b) in $\sqrt{U_{PV}h\nu}$-$h\nu$ coordinates for samples with Sn concentrations of 0%, 1%, 4%, 5% and 6%.

$$U_{PV} = U_0 \exp\left(\frac{h\nu - \varepsilon_{dir}}{E_U}\right) \quad (5)$$

where U_0 is a constant and E_U is the Urbach energy. Thus, U_{PV} decreases exponentially as the photon energy decreases in the near-bandgap region (see Fig. 5, marked area). Linear fitting of $\ln(U_{PV})$ versus the photon energy was used to extract the Urbach energy, which depends on the structural disorder of a semiconductor. Note that for semiconductors with a high degree of structural perfection, E_U lies in the range 10–20 meV, whereas for disordered or amorphous semiconductors, E_U is an order of magnitude larger [29]. For studied GeSn thin films, the derived from the PV spectra analysis value of E_U varies from 17.5 meV (sample D) to 50.8 meV (sample C) and doesn't show any correlation with Sn composition or strain. Probably, it can be influenced by some fluctuations during sample growth or dislocation density, which require further studies.

In the considered spectral range, $h\nu < \varepsilon_{dir}$, we also observed a contribution from phonon-assisted transitions in the indirect-band GeSn alloys. To highlight the indirect transitions against the background of Urbach bandtails, $\sqrt{h\nu U_{PV}}$ was plotted versus $h\nu$. When the incident photon energy was within the range $\varepsilon_{ind} < h\nu < \varepsilon_{dir}$ (Fig. 6b), linear regions were observed at the absorption edge near the indirect bandgap for films with Sn content up to 6%. For these samples, the low energy edge was attributed to indirect transitions, whereas the higher energy PV component was associated with direct transitions in the GeSn alloys. Indirect bandgap energies, ε_{ind}, were determined from extrapolation to the photon energy axis, as marked by the arrow in Fig. 6b for the $Ge_{96}Sn_4$ sample. The extracted indirect and direct bandgap energies are listed in Table 1. It can be seen that the separation difference between the direct and indirect bandgaps decreased from 92 meV for $x = 1\%$ to 42 meV for the strained $Ge_{95}Sn_5$ alloys. This decrease made it impossible to observe a contribution from the phonon-assisted indirect transitions due to their much lower probabilities compared with the direct transitions and Urbach tails.

4. Discussion

The near-bandgap optical properties of the $Ge_{1-x}Sn_x$ alloys were characterized by PV spectroscopy and SE measurements. The critical points E_0 derived from SE measurements were somewhat higher than direct bandgaps obtained from PV spectroscopy at 82 K. Similar differences between theoretical direct bandgaps and ellipsometry data were discussed previously in Refs. [3,30]. Since SE technique operates with sufficiently high intensities, the determined bandgaps may have been increased due to filling of the states near the bottom of the conduction band and top of the valence band of $Ge_{1-x}Sn_x$, i.e., a shift of the absorption edge to higher energies, known as the Burstein-Moss effect [31]. Moreover, fitting of the SE data did not take into account the compositional and strain gradient of the $Ge_{1-x}Sn_x$ films, as described previously in Ref. [20]. Thus, SE gives the effective (averaged) optical constants of films, whereas the spectral dependencies are strongly dependent on the model used for fitting the experimental data (ψ and Δ). Owing to the limitations of the SE technique near the absorption edge in spectral regions with low absorption coefficient, the critical points were shifted to higher energies as compare with direct bandgaps obtained from PV measurements. Thus, low-temperature PV spectroscopy was a more sensitive and direct technique for studying features of the absorption spectra, allowing the contributions of different types of optical transitions in the $Ge_{1-x}Sn_x$ films to be distinguished – indirect, direct as well as Urbach tails. PV spectra are measured at low excitation intensities (~μW/cm^2), as close as possible to equilibrium, which allows elimination of the shift of the absorption edge due to optical pumping. To minimize equilibrium filling of states near the bottom of the conduction band assigned to unintentional n-type doping, the measurement temperature was reduced to 82 K. Being proportional to the number of the photogenerated electron-hole pairs, i.e. to the absorption coefficient, the low-signal PV spectra reflect all critical points of dielectric function. Moreover, the PV technique is more sensitive to indirect transitions in comparison with PL measurements that requires sufficient quantum yield or direct transmission measurements limited by low absorptivity of thin film.

It was observed that as the Sn content increased, the absorption edge shifts toward lower energy due to changes in the electronic band structure of GeSn alloys. As follows from XRD measurements, the $Ge_{1-x}Sn_x$ films with x up to 12% had a nearly uniform content, enabling their bandgaps to be determined by PV or SE studies. At the same time, thick films with a Sn content of 12% were found to be two-layered. Fig. 7 shows the near-bandgap PV spectra of $Ge_{88}Sn_{12}$ films with different thickness (45 nm, 100 nm, 150 nm and 200 nm) measured at 82 K and plotted in $(h\nu U_{PV})^2$-$h\nu$ coordinates. Two linear regions, indicating the presence of two separate direct

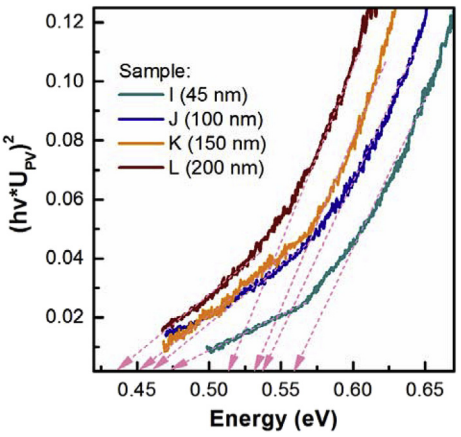

Fig. 7. Near-bandgap photovoltage spectra of GeSn films with 12% Sn and different thickness measured at 82 K.

transitions in the $Ge_{1-x}Sn_x$ films, were observed for these samples. Note that owing to a strong impact of surface recombination on PV, the contribution of electron-hole pairs photogenerated in the top layer was lower in comparison with the PV component attributed to the bottom layer of $Ge_{1-x}Sn_x$. As each PV component was a straight line on the $(h\nu U_{PV})^2$-$h\nu$ plot, they gave the direct bandgaps of two sublayers of $Ge_{1-x}Sn_x$ with different x. As the thickness increased, the edge of PV spectra shifted toward lower energy due to formation of a Sn-rich top layer and strain relaxation. As follows from XRD measurements, both a decrease of strain and increase of Sn content were observed for the top layer. The difference in lattice constants of these sublayers was sufficient to observe double Bragg peaks from $Ge_{1-x}Sn_x$ for samples K and L only. For instance, the PV spectra of samples L with 200 nm films (see Fig. 7) contained a low energy PV component with threshold energy near 423 meV associated with absorption in the Sn-rich $Ge_{85.1}Sn_{14.9}$ top layer. The predicted direct bandgap for the layer with $x = 14.9\%$ and compressive strain of −0.809% was found to be near 406 meV, whereas the strained $Ge_{88}Sn_{12}$ (−1.49%) had a direct bandgap of 496 meV at 300 K. The Sn content in the bottom $Ge_{88}Sn_{12}$ layer was found to be the same for all samples, while the strain decreased from −1.49% for sample I to −0.36% for sample L (Table 1). Therefore, the direct bandgap for the $Ge_{88}Sn_{12}$ layer decreased from 543 meV to 505 meV due to strain relaxation. Within this range of strain values, indirect-to-direct transitions are likely to occur for the $Ge_{88}Sn_{12}$ alloys. Previously published calculation of the electronic band structure using the 8-band k·p method for compressively strained $Ge_{87.5}Sn_{12.5}$ alloys showed that the transitions to a direct bandgap were expected near ε_{xx} ~1% [32].

The direct bandgaps were determined from extrapolation to the photon energy axis, which allowed analysis of the compositional dependence of the direct bandgap of strained $Ge_{1-x}Sn_x$ alloys up to 14.9% at 82 K. A red shift of the bandgap was observed as the Sn concentration increased, in good agreement with previously published data [33] and energies calculated from the following widely used polynomial:

$$\varepsilon^{R}_{\mathrm{ind,dir}} = xE^{L,\Gamma}_{g,\mathrm{Sn}} + (1-x)E^{L,\Gamma}_{g,\mathrm{Ge}} - b^{L,\Gamma}_{\mathrm{GeSn}}x(1-x), \quad (6)$$

where $E^{\Gamma}_{g,\mathrm{Ge}} = 0.838$ eV, $E^{\Gamma}_{g,\mathrm{Sn}} = -0.413$ eV, $E^{L}_{g,\mathrm{Ge}} = 0.734$ eV and $E^{L}_{g,\mathrm{Sn}} = 0.006$ eV are the direct and indirect bandgaps at 82 K for the crystalline Ge and Sn, correspondingly, and $b^{L,\Gamma}_{\mathrm{GeSn}}$ is the bowing factor for the indirect (b^{L}_{GeSn}) or direct ($b^{\Gamma}_{\mathrm{GeSn}}$) bandgap of the $Ge_{1-x}Sn_x$ alloy [7,34]. Besides the bandgaps of Ge and Sn, accurate determination of the bowing factors is important for prediction of the indirect and direct bandgaps of $Ge_{1-x}Sn_x$ over a wide composition range. Experimentally determined values of $b^{\Gamma}_{\mathrm{GeSn}}$ were reported to be in the range 1.8 eV–2.8 eV [35–38], whereas first principle calculations gave values of 1.9 eV [39], 2.06 eV [40] and 2.55 eV [41]. In order to describe the compositional dependence of the direct bandgap over a broad range of Sn content, a non-constant or compositional dependent bowing factor (2.66–5.4x) was proposed [32]. Conversely, the bowing factor for the bandgap at the L-point of the Brillouin zone is much less studied. Indirect bandgap bowing of 0.8 eV or 0.17 eV at 10 K was determined experimentally from PL spectroscopy depending on whether the phonon emission energy was taken into account [42]. Room temperature PL spectroscopy gave $b^{L}_{\mathrm{GeSn}} = 1.03$ eV [7], whereas measurements over a broader compositional range exceeding 10% led to a non-constant bowing factor of 1.11–0.78x eV [33]. In contrast, the simulated value of b^{L}_{GeSn} reported in Ref. [43] was 0.89 eV. This difference is likely due to difficulties in the experimental determination of the bowing factor for the bandgap at the L-point for a wide range of x. Besides the decreasing energy difference between the L- and Γ-valleys as the Sn content increases, optical measurements of indirect bandgaps are complicated by the need to take account of the energy of phonons involved in the indirect transitions and the Burstein-Moss effect, which shifts the effective absorption edge to higher energies [31,43].

To compare calculated indirect and direct bandgaps with experimentally determined values, we considered the strain-induced shifts of the conductive band and valence band edges under the assumption of coherently strained $Ge_{1-x}Sn_x$ alloys and following the procedure described in detail in Ref. [44]. The direct ($\varepsilon^{str}_{\mathrm{dir}}$) and indirect ($\varepsilon^{str}_{\mathrm{ind}}$) bandgaps in the compressive strained $Ge_{1-x}Sn_x$ were simulated as follows:

$$\varepsilon^{str}_{\mathrm{dir}} = \varepsilon^{R}_{\mathrm{dir}} + \left(a^{\Gamma}_{C} - a_V\right)\left(2\varepsilon_{\parallel} + \varepsilon_{\perp}\right) + b_S\left(\varepsilon_{\perp} - \varepsilon_{\parallel}\right), \quad (7)$$

$$\varepsilon^{str}_{ind} = \varepsilon^{R}_{\mathrm{ind}} + \left(a^{L}_{C} - a_V\right)\left(2\varepsilon_{\parallel} + \varepsilon_{\perp}\right) + b_S\left(\varepsilon_{\perp} - \varepsilon_{\parallel}\right), \quad (8)$$

where $\varepsilon_{\perp} = -2(C_{12}/C_{11})\varepsilon_{\parallel}$ (for (001) oriented films), a_V, $a^{\Gamma,L}_{C}$ is the hydrostatic deformation potential of the valence band and conduction band, b_S is the shear deformation potential. The hydrostatic and shear deformation potentials for Ge are given by $a_V = 1.24$ eV, $a^{\Gamma}_{C} = -8.24$ eV, $a^{L}_{C} = -1.54$ eV, $b_S = -2.9$ eV, respectively. Consequently, $a_V = 1.58$ eV, $a^{\Gamma}_{C} = -6.00$ eV, $a^{L}_{C} = -2.14$ eV, $b_S = -2.7$ eV are the deformation potentials of α-Sn, respectively. Sets of deformation potentials for Ge and α-Sn were chosen in the same way as described in Ref. [45]. All deformation potentials and structural parameters for $Ge_{1-x}Sn_x$ alloys were interpolated according to Vegard's law.

In order to determine the bowing parameter, we have analyzed the experimental data points derived from PV measurements, comparing them with calculated bandgaps for fully strained $Ge_{1-x}Sn_x$ alloys. The procedure involves the calculation of bandgaps for the relaxed films taking into account the bowing parameter. Then, the bandgaps of the fully strained $Ge_{1-x}Sn_x$ alloys was calculated and compared with the experimental data points. As a result, we have find the value of the bowing parameter by minimizing the standard deviation in the range 0–12% of Sn. Note that being determined from PV measurements of partially strained films, a systematic error of about 20% is introduced in the direct bandgaps for the alloys with Sn content higher than x ~12% due to strain relaxation. As for bowing parameter for indirect bandgaps,

the analyzed range 0–6% of Sn covers only the data points determined for the unrelaxed $Ge_{1-x}Sn_x$.

The best fits with $b^{\Gamma}_{GeSn} = 3.16–0.5x$ and $b^{L}_{GeSn} = 1.93$ eV for the direct and indirect bandgaps of fully strained $Ge_{1-x}Sn_x$, respectively, yielded the experimentally determined values presented in Fig. 8. The crossover point for the relaxed alloys was found to be around 6%. According to the simulations, the crossover point was not observed for coherently strained $Ge_{1-x}Sn_x$ over the studied range of Sn compositions with the given bowing factors. However, assumption of a composition dependent b^{L}_{GeSn} will make significant corrections. Specifically, the bandgap values depend strongly on the bowing factor used for calculation, especially at high Sn content. For instance, assuming $b^{L}_{GeSn} = 1.03$ eV and $b^{\Gamma}_{GeSn} = 2.46$ eV [7], the crossover point is expected near 20% and 7.3% for the coherently strained and relaxed GeSn, whereas using $b^{L}_{GeSn} = 0.26$ eV and $b^{\Gamma}_{GeSn} = 2.2$ eV shifts this point to 11% and 5.7%, respectively [45]. Therefore, experimental determination of indirect bandgaps over a broad range is required for accurate specification of the crossover point of the strained $Ge_{1-x}Sn_x$.

Our films were slightly relaxed, with strain values increasing linearly with increasing Sn content up to $x = 12\%$. Further estimations based on strain values derived from XRD analysis showed that observation of the crossover point was not possible for the studied range of Sn content due to compressive strain. The experimental indirect and direct bandgaps of GeSn probed by PV spectroscopy were in good agreement with data calculated from Eq. (8) over the composition range $0 < x < 6\%$. We could not distinguish the contribution of indirect transitions against the background for higher x due to the dominant contribution of direct transitions and Urbach tailing. Furthermore, interpolation of the experimental values for the direct and indirect bandgaps gave no evidence in favor of the observation of crossover up to 12% in the studied films. It is well known that achievement of a crossover point requires low strain in $Ge_{1-x}Sn_x$ alloys, whereas an indirect-to-direct transition is not possible in the coherently strained $Ge_{1-x}Sn_x$ alloys for the considered range of Sn content. However, as reported previously [46], films of thickness beyond a critical value (about 50 nm) plastically relax via formation of misfit dislocations. For the example of structures with $Ge_{88}Sn_{12}$ alloys, presented in Fig. 6b, we observed a shift of the absorption edge to lower energies due to relaxation as the film thickness increased. According to our experiments, for films with a Sn content of 12%, an increase in the film thickness led not only to the relaxation of strain but also formation of a relaxed top layer of $Ge_{1-x}Sn_x$ film with higher Sn content, and hence smaller bandgap. This effect is useful for designing tandem solar cells and broadband IR photodetectors.

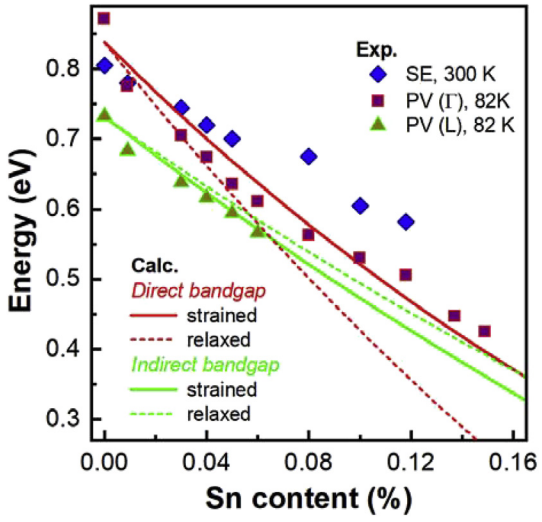

Fig. 8. Direct and indirect band gap energies extracted from photovoltage spectra measured at 82 K. The curves show calculated values of direct and indirect bandgaps for coherently strained GeSn films with $b^{\Gamma}_{GeSn} = 3.16–0.5x$ and $b^{L}_{GeSn} = 1.93$ eV. The dash lines correspond to bandgaps calculated for relaxed $Ge_{1-x}Sn_x$ films at 82 K.

5. Conclusions

In summary, the near-bandgap optical properties of strained $Ge_{1-x}Sn_x$ films grown on Ge were characterized by PV spectroscopy and SE measurements. Contributions of Urbach tailing and direct and indirect optical transitions were observed. The experimental direct and indirect bandgaps were compared with calculations based on a widely used polynomial that assumes variation of the electronic band structure between Ge and Sn taking into account the strain-related shifts for the conduction and valence bands. It was shown that the compositional dependence of the direct bandgaps of the strained $Ge_{1-x}Sn_x$ films derived from PV measurements at 82 K could be described by a non-constant bowing factor $b^{\Gamma}_{GeSn} = 3.16–0.5x$ for the Γ-point of the Brillouin zone in the range from 0% to 12% Sn content. In contrast to SE, low-temperature PV spectroscopy of GeSn alloys with x up to 6% was able to distinguish the contribution of indirect optical transitions at lower energies than direct transitions and determine the bandgaps at the Γ- and L-point. Because of the narrower range of Sn content, use of a constant bowing factor $b^{L}_{GeSn} = 1.93$ eV was found to be sufficient for good agreement between the experimental and calculated indirect bandgaps. As the Sn composition increased for $x > 6\%$, the difference between the energies of the indirect and direct bandgaps decreased to such an extent that it became impossible to identify the indirect bandgap energies against the background contribution of direct transitions and Urbach tailing. According to the simulations, the crossover point was not achieved using the given bowing factors for the coherently strained $Ge_{1-x}Sn_x$ alloys with the studied range of Sn compositions. Therefore, experimental determination of indirect bandgaps over a broader range of Sn up to 15% is required for more accurate specification of the crossover point of strained $Ge_{1-x}Sn_x$ alloys.

This work shows that the measured indirect and direct bandgaps by photovoltage spectroscopy are in good agreement with theoretically predicted by using conventional deformation potential. As follows from determined compositional dependencies of the bandgaps at the Γ- and L-points, operating wavelength of $Ge_{1-x}Sn_x$ based direct-bandgap optoelectronic devices can be extended to the mid-infrared range if the compressive strain and alloy composition inhomogeneities will be reduced.

Acknowledgment

The authors acknowledge the financial support by the National Science Foundation of the U.S. grant 1809054/QUANTUM INTERFACES. Dr. Yu also acknowledges support from the Air Force Office of Scientific Research under grant FA9550-14-1-0205.

Appendix A. Supplementary data

Supplementary data to this article can be found online at https://doi.org/10.1016/j.actamat.2019.04.004.

References

[1] Physics of Group IV Elements and III–V Compounds, Landolt-Börnstein: Numerical Data and Functional Relationships in Science and Technology; Berlin,

Germany, vol. 17a, 1982.
[2] S. Gupta, B. Magyari- Köpe, Y. Nishi, K.C. Saraswat, J. Appl. Phys. 113 (2013), 073707.
[3] V.R. D'Costa, C.S. Cook, A.G. Birdwell, C.L. Littler, M. Canonico, S. Zollner, J. Kouvetakis, J. Menendez, Phys. Rev. B 73 (2006) 125207.
[4] Y. Ishikawa, K. Wada, D.D. Cannon, J. Liu, H.-C. Luan, L.C. Kimerling, Appl. Phys. Lett. 82 (2003) 2044–2046.
[5] J. Mathews, R.T. Beeler, J. Tolle, C. Xu, R. Roucka, J. Kouvetakis, J. Menendez, Appl. Phys. Lett. 97 (2010) 221912.
[6] C. Eckhardt, K. Hummer, G. Kresse, Phys. Rev. B 89 (2014) 165201.
[7] L. Jiang, J.D. Gallagher, C.L. Senaratne, T. Aoki, J. Mathews, J. Kouvetakis, J. Menendez, Semicond. Sci. Technol. 29 (2014) 115028.
[8] L. Liu, R. Liang, J. Wang, J. Xu, AIP Adv. 6 (2016), 015102.
[9] H. Ladrón de Guevara, A. Rodrıguez, H. Navarro-Contreras, M. Vidal, Appl. Phys. Lett. 84 (2004) 4532–4534.
[10] F. Ratto, F. Rosei, A. Locatelli, S. Cherifi, S. Fontana, S. Heun, P.-D. Szkutnik, A. Sgarlata, M. De Crescenzi, N. Motta, Appl. Phys. Lett. 84 (2004) 4526–4528.
[11] H. Lin, R. Chen, W. Lu, Y. Huo, T.I. Kamins, J.S. Harris, Appl. Phys. Lett. 100 (2012) 102109.
[12] M. Medikonda, G.R. Muthinti, R. Vasić, T.N. Adam, A. Reznicek, M. Wormington, G. Malladi, Y. Kim, Y.-C. Huang, A.C. Diebold, J. Vac. Sci. Technol. B 32 (2014), 061805.
[13] V.R. D'Costa, W. Wang, Y.-C. Yeo, J. Appl. Phys. 120 (2016), 063104.
[14] A.V. Maslov, V.N. Astratov, Appl. Phys. Lett. 108 (2016), 051104.
[15] W. Du, S.A. Ghetmiri, B.R. Conley, A. Mosleh, A. Nazzal, R.A. Soref, G. Sun, J. Tolle, J. Margetis, H.A. Naseem, S.-Q. Yu, Appl. Phys. Lett. 105 (2014), 051104.
[16] S.Q. Yu, S.A. Ghetmiri, W. Du, J. Margetis, Y. Zhou, A. Mosleh, S. Al-Kabi, A. Nazzal, G. Sun, R.A. Soref, J. Tolle, B. Li, H.A. Naseem, Proc. V. 9367, Silicon Photonics X (2015) 9670R.
[17] J.Tolle, U.S. patent 20,140,087,544 (27 March 2014)..
[18] W. Dou, M. Benamara, A. Mosleh, J. Margetis, P. Grant, Y. Zhou, S. Al-Kabi, W. Du, J. Tolle, B. Li, M. Mortazavi, S.-Q. Yu, Sci. Rep. 8 (2018) 5640.
[19] J. Margetis, A. Mosleh, S.A. Ghetmiri, S. Al-Kabi, W. Dou, W. Du, N. Bhargava, S.-Q. Yu, H. Profijt, D. Kohen, R. Lood, A. Vohrad, J. Tolle, Mater. Sci. Semicond. Process. 70 (2017) 38.
[20] J. Margetis, S.-Q. Yu, B. Li, J. Tolle, J. Vac. Sci. Technol. A 37 (2019), 021508.
[21] S. Assali, J. Nicolas, S. Mukherjee, A. Dijkstra, O. Moutanabbir, Appl. Phys. Lett. 112 (2018) 251903.
[22] C. Xu, C.L. Senaratne, R.J. Culbertson, J. Kouvetakis, J. Menéndez, J. Appl. Phys. 122 (2017) 125702.
[23] N. Bhargava, M. Coppinger, J.P. Gupta, L. Wielunski, J. Kolodzey, Appl. Phys. Lett. 103 (2013), 041908.
[24] N.S. Fernando, R.A. Carrasco, R. Hickey, J. Hart, R. Hazbun, S. Schoeche, J.N. Hilfiker, J. Kolodzey, S. Zollner, J. Vac. Sci. Technol. B Nanotechnol. Microelectron. 36 (2018), 021202.
[25] B. Johs, C.M. Herzinger, J.H. Dinan, A. Cornfeld, J.D. Benson, Thin Solid Films 313–314 (1998) 137–142.
[26] H. Tompkins, E.A. Irene, Handbook of Ellipsometry, William Andrew, 2005.
[27] M. Cardona, Modulation Spectroscopy, Academic press, New York, 1969.
[28] S.M. Sze, K.K. Ng, Physics of Semiconductor Devices, Wiley-Interscience, Hoboken, New Jersey, 2006.
[29] G.D. Cody, J. Non-Cryst. Solids 141 (1992), 3-1.
[30] M.P. Polak, P. Scharoch, R. Kudrawiec, J. Appl. Phys. 50 (2017) 195103.
[31] E. Burstein, Phys. Rev. 93 (1954) 632. T. S. Moss, Proc. Phys. Soc. B 67, 775 (1954).
[32] D. Stange, S. Wirths, N. von den Driesch, G. Mussler, T. Stoica, Z. Ikonic, J.M. Hartmann, S. Mantl, D. Grützmacher, D. Buca, ACS Photonics 2 (2015) 1539–1545.
[33] A. Gassenq, L. Milord, J. Aubin, K. Guilloy, S. Tardif, N. Pauc, J. Rothman, A. Chelnokov, J.M. Hartmann, V. Reboud, V. Calvo, Appl. Phys. Lett. 109 (2016) 242107.
[34] J.D. Gallagher, C.L. Senaratne, J. Kouvetakis, J. Menéndez, Appl. Phys. Lett. 105 (2014) 142102.
[35] K. Zelazna, M.P. Polak, P. Scharoch, J. Serafinczuk, M. Gladysiewicz, J. Misiewicz, J. Dekoster, R. Kudrawiec, Appl. Phys. Lett. 106 (2015) 142102.
[36] H. Lin, R. Chen, W. Lu, Y. Huo, T.I. Kamins, J.S. Harris, Appl. Phys. Lett. 100 (2012) 102109.
[37] H.P.L. de Guevara, A.G. Rodríguez, H. Navarro-Contreras, M.A. Vidal, Appl. Phys. Lett. 91 (2007) 161909.
[38] G. He, H. Atwater, Phys. Rev. Lett. 79 (1997) 1937–1940.
[39] Y. Chibane, M. Ferhat, J. Appl. Phys. 107 (2010), 053512.
[40] Y. Chibane, B. Bouhafs, M. Ferhat, Phys. Status Solidi B 240 (2003) 116–119.
[41] W.-J. Yin, X.-G. Gong, S.-H. Wei, Phys. Rev. B 78 (2008), 161203(R).
[42] A.A. Tonkikh, C. Eisenschmidt, V.G. Talalaev, N.D. Zakharov, J. Schilling, G. Schmidt, P. Werner, Appl. Phys. Lett. 103 (2013), 032106.
[43] P. Piquini, A. Zunger, Phys. Rev. B 78 (2008), 161302(R).
[44] C.G. Van de Walle, Phys. Rev. B 39 (1989) 1871–1883.
[45] H.S. Mączko, R. Kudrawiec, M. Gladysiewicz, Sci. Rep. 6 (2016) 34082.
[46] N. Von den Driesch, D. Stange, S. Wirths, G. Mussler, B. Holländer, Z. Ikonic, J.M. Hartmann, T. Stoica, S. Mantl, D. Grützmacher, D. Buca, Chem. Mater. 27 (2015) 4693–4702.